Multidimensional adaptive radar array processing using an iterative optical matrix-vector processor

David Casasent
Mark Carlotto*
Carnegie-Mellon University
Department of Electrical Engineering
Pittsburgh, Pennsylvania 15213

Abstract. An iterative optical matrix-vector processor that computes the adaptive weights for a phased array radar is described. Multidimensional adaptivity in both target angle and velocity is achieved by lexicographically ordering the antenna elements as they are fed to the optical processor. Complex weights are computed by spatial multiplexing of the vector and matrix inputs to the system. The error sources of the optical system and the convergence of the iterative algorithm are analyzed, and experimental demonstration of the accuracy and performance of the system is included. This novel processor is found to perform quite adequately and to be most appropriate for advanced multidimensional adaptive phased array radars.

Keywords: two-dimensional signal processing; multidimensional adaptivity; radar array processing; iterative optical matrix-vector processor; adaptive phased array signal processing; angle adaptivity.

Optical Engineering 21(5), 814-821 (September/October 1982).

CONTENTS

1. INTRODUCTION

Adaptive phased array radar (APAR)[1-3] represents a formidable signal processing problem of considerable current interest[4,5] and one for which advanced signal processing concepts and algorithms are necessary. The real-time and parallel processing features of optical systems make them attractive candidates for this application. However, the nature of the APAR problem requires a new optical processing system that performs more general functions besides the Fourier transform and correlation operations normally realized in such systems.[6] In this paper, we describe a new and general purpose optical processor, discuss its application for APAR processing, provide experimental demonstrations of its use in APAR processing, and analyze the accuracy and performance of the system for this application.

In Sec. 2, we describe the APAR signal processing problem. Computation of the optimum set of adaptive weights to apply to the receiving elements of the antenna to steer it in a desired direction and to null all noise sources in other directions is formulated as the solution of a matrix-vector equation requiring the inversion of a matrix. In Sec. 3, we describe an iterative optical matrix-vector processor (IOP) that we have fabricated[7] to address this problem.[8] We also discuss how complex values are accommodated on this system and how convergence of the iterative algorithm is achieved. We also advance an error source model for the processor. The experimental use of the IOP to cancel noise sources distributed in angle is then demonstrated in Sec. 4. In Sec. 5, we extend our theory to the case of multidimensional adaptive antennas. Experimental demonstration of the use of the IOP for an antenna adaptive in both space and time is included in Sec. 6 together with an initial error source and accuracy analysis of this new optical processor for this application.

2. ADAPTIVE PHASED ARRAY SIGNAL PROCESSING

For simplicity, we initially consider a linear phased array antenna with adaptive steering and noise null cancellation in angle (θ) only. In Sec. 5, we extend this theory to the case of multidimensional adaptive antennas. Consider the linear (1-D) phased array antenna system of Fig. 1 with N isotropic elements spaced $d = \lambda_R/2$ apart (where λ_R is the wavelength of the radar). In the far field of the antenna (i.e., at ranges $R \gg (Nd)^2/\lambda_R$), we assume a signal $s(t)\exp(j\omega t)$ at an angle θ_0 (this represents the direction in which we wish to steer the antenna and obtain maximum response) and M uncorrelated, zero-mean, narrow-band interference sources $r_m(t)$

*Present address: The Analytical Sciences Corporation, 1 Jacob Way, Reading, MA 01867.

Invited Paper TD-102 received Apr. 27, 1982; revised manuscript received May 18, 1982; accepted for publication May 21, 1982; received by Managing Editor June 1, 1982.

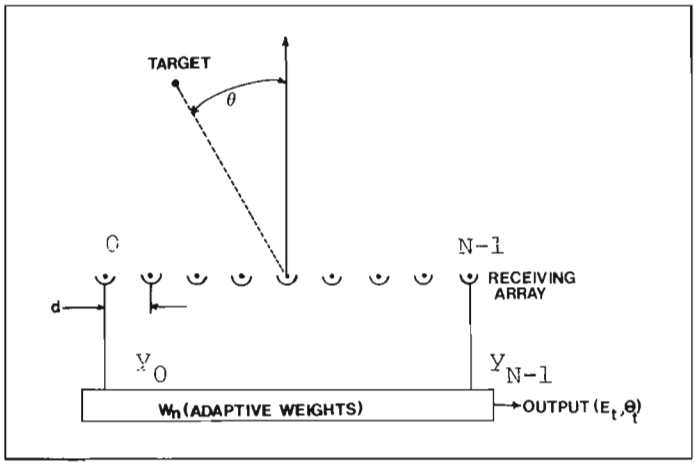

Fig. 1. Simplified pictorial block diagram of an adaptive phased array radar processor.

$\exp(j\omega t)$ at angles $\theta_1, \ldots, \theta_M$. All angles are measured with respect to boresight (the normal to the array). The objective of an APAR is to point the antenna in the direction θ_0 and to null the antenna pattern in the directions θ_m of the interference sources. With the signal and interference sources in the far field of the antenna, the radiation incident on the array can be described by the superposition of plane waves from the directions of each source. Since the path difference between two antenna elements is $d \sin\theta = (\lambda_R \sin\theta)/2$, the signal received at the n-th antenna element is

$$z_n(t) = s(t)\, e^{j(\omega t + \pi n \sin\theta_0)} + \sum_{m=1}^{M} r_m(t)\, e^{j(\omega t + \pi n \sin\theta_m)} . \quad (1)$$

Each of these N antenna outputs, $\underline{z}(t) = \{z_n(t)\}$, is multiplied by a complex weight $\underline{w} = \{w_n\}$, and the output from the receiver is the coherent summation of the products of the weights and the received signals:

$$v_{out}(t) = \sum_{n=0}^{(N-1)} w_n z_n(t) = \underline{w}^T \underline{z}(t) . \quad (2)$$

In Eq. (2) and in our future descriptions, we employ vector and matrix notation to describe the various signal components of the system. Lower (upper) case letters with an underbar denote vectors (matrices).

The antenna pattern that is obtained from such a receiver is described by an angular response $E(\theta)$ which is the inverse Fourier transform of the weighting pattern $\{w_n\}$. The attractive feature of a phased array radar is the ease with which one can steer the antenna. To direct the antenna to $\theta = \theta_0$, we simply weight the antenna outputs by the conjugate phase pattern $w_n = \exp(-j\pi n \sin\theta_0)$. When uncorrelated noise is present, due to uniform background radiation or thermal noise in the antenna itself, this weighting maximizes the signal-to-noise power ratio (SNR) at the antenna's output.[2] However, when directional interference is present, this simple weighting is not optimal, and the weights must be computed adaptively as a function of the changes in the rf noise environment. This is the APAR signal processing problem with which we are concerned. In Ref. 9, we show that the vector $\underline{w}$ which minimizes the mean square error between the signal and array output satisfies the matrix-vector equation

$$\underline{M}\,\underline{w} = P_0 \underline{s}^* , \quad (3)$$

where $\underline{M} = \overline{\underline{z}^*(t)\underline{z}^T(t)}$ the covariance matrix of the received signal plus interference; $P_0 = \overline{s^*(t)\, s(t)}$ the signal power; $\underline{s} = \exp(j\pi n \sin\theta_0)$ is the steering vector. In Ref. 9, we also show that the solution $\underline{w}$ to Eq. (3) also maximizes the SNR at the output of the antenna. These results are in agreement with the conclusions in Refs. 1, 2, and 4.

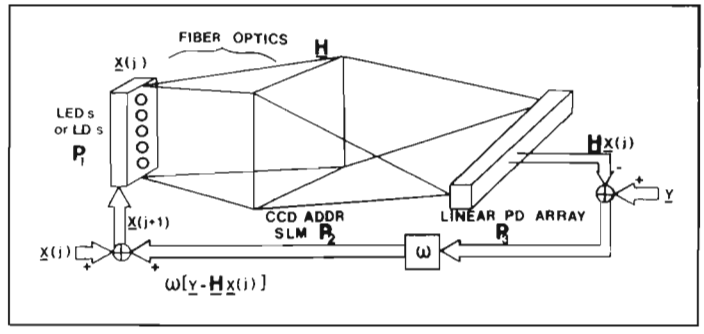

Fig. 2. Schematic diagram of the iterative optical matrix-vector processor.[7]

3. ITERATIVE OPTICAL PROCESSOR

From Sec. 2, we found that the solution of the optimal adaptive weights $\underline{w}$ that will steer an antenna in a direction $\underline{s}^*$ and null directional interference noise described by the covariance matrix $\underline{M}$ must satisfy the vector-matrix equation

$$\underline{M}\,\underline{w} = \underline{s}^* . \quad (4)$$

The constant multiplicative factor P_0 in Eq. (3) does not affect the computed solution $\underline{w}$. In Refs. 7–10, we described an iterative optical processor (IOP) that can solve matrix-vector equations or systems of linear algebraic equations such as Eq. (4). An improved version of this IOP is shown schematically in Fig. 2. The input at P_1 is a linear array of LEDs or laser diodes (LDs), whose outputs at time j describe a vector $\underline{x}(j)$. This vector output is imaged vertically and expanded horizontally to uniformly illuminate row m of P_2 with the input x_m. A 2-D mask whose transmittance is described by a matrix $\underline{H}$ is placed at P_2. The light distribution leaving each column of $\underline{H}$ is collected on a separate photodetector at P_3. The output from the linear photodetector array at P_3 is thus the matrix-vector product $\underline{H}\underline{x}(j)$.

With such a matrix-vector processor (as described in Refs. 11, 12 and more recently in Ref. 13) as the basic element of our system, we subtract an external vector $\underline{y}$ from $\underline{H}\underline{x}(j)$, multiply the difference by a constant acceleration parameter ω, and add the result to the prior $\underline{x}(j)$ input to obtain a new iterative input $\underline{x}(j+1)$ for time $j+1$. This IOP thus realizes the Richardson algorithm[14] in the form

$$\underline{x}(j+1) = \underline{x}(j) + \omega\left[\underline{H}\underline{x}(j) - \underline{y}\right] . \quad (5)$$

When $\underline{x}(j) = \underline{x}(j+1) = \underline{x}$, Eq. (5) reduces to

$$\underline{H}\underline{x} = \underline{y} , \quad (6)$$

and the system's output is

$$\underline{x} = \underline{H}^{-1}\underline{y} \quad (7)$$

or the solution of the matrix-vector equation in Eq. (6). Such a system can be directly used for the APAR problem described in Sec. 2 and summarized in Eq. (4). We simply use the covariance matrix $\underline{M}$ as the matrix $\underline{H}$, the steering vector $\underline{s}^*$ as the exogenous vector $\underline{y}$, and the solution vector $\underline{x}$ is then the desired set of adaptive weights $\underline{w}$ to be computed.

In Ref. 7, we detailed the fabrication and performance of the laboratory IOP system we assembled. As the inputs, we used ten LEDs which were interconnected to the mask by a fiber optic system. A film transparency is used as the mask in our present laboratory system, although a real-time 2-D light modulator such as the CCD-addressed liquid crystal light valve[15] can provide a real-time adaptive

mask for this system. Alternatively, a new optical systolic array architecture[16] using a 1-D acousto-optic cell at P_2 of Fig. 2 with feedback of the photodetector outputs to the acousto-optic cell's inputs[17] can also be used to provide a fully real-time iterative optical matrix-vector processor. For now, we consider only the system of Fig. 2. The height of the matrix mask used at P_2 is 4 mm, and it was chosen to match the height of the detector elements in our linear photodetector array at P_3. We also chose the horizontal spacings between detector elements, and thus, in our present system, we simply place the output photodetector array in direct contact with the mask at P_2.

Since the outputs from the LEDs and the transmittances of the mask elements are real and positive, this system can multiply and add only positive numbers. In the APAR problem, the elements of the matrices and vectors are complex valued. Thus, to provide the complex-valued matrix-vector product in Eq. (4), we employ spatial and temporal multiplexing. We realize a bipolar matrix-vector product $\underline{y} = \underline{H}\underline{x}$ by scaling, biasing, and partitioning $\underline{H}$ such that it is a unipolar matrix. We then operate the IOP twice. On the first cycle, the positive values $\underline{x}_1$ of $\underline{x}$ are the inputs, and on the second cycle the negative values $\underline{x}_2$ of $\underline{x}$ are the LED inputs. In the postprocessor, we form the difference $\underline{H}\underline{x}_1 - \underline{H}\underline{x}_2$ of the two successive matrix-vector outputs and scale and bias the result to provide the new inputs for the next iterative cycle. This procedure is detailed in Ref. 7, where we discuss how this procedure reduces the required space bandwidth product of the mask and enables all fixed pattern detector noise to be canceled. To enable the system to perform complex-valued matrix-vector multiplications, we partition the matrix and the vectors in the system as

$$\underline{y} = \begin{bmatrix} \underline{s}^*_{re} \\ \underline{s}^*_{im} \end{bmatrix}, \quad \underline{H} = \begin{bmatrix} \underline{M}_{re} & -\underline{M}_{im} \\ \underline{M}_{im} & \underline{M}_{re} \end{bmatrix}, \quad \underline{x} = \begin{bmatrix} \underline{w}_{re} \\ \underline{w}_{im} \end{bmatrix}, \tag{8}$$

where the subscripts re and im denote the bipolar real and imaginary parts of the indicated vectors and matrices. To accommodate complex-valued matrix-vector operations on the system, we bias $\underline{M}$, form a unipolar matrix as before, partition it as indicated in Eq. (8), format the vectors $\underline{x}$ and $\underline{y}$ as in Eq. (8), and operate the system for two cycles with the positive- and negative-valued vector elements as the inputs. We detail this complex-valued algorithm and demonstrate its use for a specific example in Sec. 6. In Sec. 4, we describe an alternate complex-valued algorithm and demonstrate its use on the IOP system of Fig. 2.

A new feature included in the system of Fig. 2 is the presence of the acceleration parameter ω. (We retain the standard notation ω for the acceleration factor. This will cause no confusion with the radian frequency ω in practice.) Proper selection of ω ensures convergence of the iterative algorithm and speeds the convergence, as we now discuss. Since $\underline{M}$ is a positive definite Hermetian matrix, its N eigenvalues λ_n are positive, and thus to ensure convergence of Eq. (5), we require ω to satisfy[7]

$$|1 - \omega\lambda_n| < 1. \tag{9}$$

This is ensured by the choice[7]

$$\omega = ||\underline{H}||^{-1} = \left(\sum_m \sum_n h_{mn}^2 \right)^{-1/2}, \tag{10}$$

where the Euclidean norm of $\underline{H}$ (the square root of the sum of the squares of the elements h_{mn} of $\underline{H}$) is represented by the symbol shown. When the spatial multiplexing in Eq. (8) is used, $||\underline{H}|| = \sqrt{2}||\underline{M}||$ is used in Eq. (10).

The accuracy and performance obtainable for any analog or optical processor is an issue of primary concern. In the error source model we have developed for the IOP, we separate the errors of the system into spatially-fixed and temporal errors. In terms of these errors, we describe the observed output $\hat{\underline{z}} = \underline{H}\underline{x}$ obtained from the matrix-vector multiplier as the exact result $\underline{z}_{exact}$ plus two terms:

$$\hat{\underline{z}} = \underline{z}_{exact} + \underline{z}_{spatial} + \underline{z}_{temporal}. \tag{11}$$

The spatially fixed errors in the IOP are due to nonuniformity and nonlinearity in the LED and detector responses, spatial variations in the transmittances of the fiber optic interconnections, and errors in the transmittances of the elements of the mask. We can correct for the source and detector errors by multiplying the inputs to the LEDs by a fixed correction vector stored in read-only memory. The residual spatial nonuniformities that remain can all be transferred to the mask plane. This is quite attractive since we can then correct for all residual spatial errors by properly modifying the matrix data as they are recorded on the mask. For our laboratory system, the measured residual spatial error without a correction mask was $\pm 0.8\%$.[7] This represents $\underline{z}_{spatial}$ in Eq. (11) under uniform LED illumination. Since it is adequate for our applications, as we will see, no further corrections for it were included in our present system. The temporal time-varying component of the system noise $\underline{z}_{temporal}$ in Eq. (11) is due to the detector. It was measured to be $\pm 0.4\%$ for our system. As before, this is sufficiently small that cooled detectors and other measures to decrease this noise component were not used. This latter error source represents the fundamental limit and performance of the IOP. In Sec. 6, we use our error source model in Eq. (11) and present an initial analysis (with experimental confirmation) of the performance of the IOP for a multidimensional adaptive antenna.

4. ANGLE ADAPTIVITY USING THE IOP

As an initial example of the use of the IOP for APAR processing, we consider interference sources distributed only in angle as described in Sec. 2. We also use this initial example to detail an alternate method to process complex-valued data on the IOP. We consider a two-element array with one interference source at an angle θ_1 with noise power P_1 (per received channel) and with additive receiver noise of N_r watts per channel. We ignore the signal strength in this present treatment. The received signals at the two array elements are

$$z_1 = x_1 + y_1 ;$$
$$z_2 = x_2 + y_2 , \tag{12}$$

where x_n and y_n are the interference voltage and noise voltage in channel n. The voltage x_2 will lag x_1 by a phase angle $\gamma = \pi \sin\theta_1$ (where $d = \lambda_R/2$ is assumed), and the noise voltages y_n will be independent of each other and of the x_n signals. For this case, the covariance matrix is

$$\underline{M} = \begin{bmatrix} P_1 + N_r & P_1 \exp(-j\gamma) \\ P_1 \exp(+j\gamma) & P_1 + N_r \end{bmatrix}. \tag{13}$$

In this initial experiment,[8] we set $\omega = 1$ in Eq. (5), and to avoid the need to add the original input to the difference between the matrix-vector product and the exogenous vector, we place $[\underline{I} - \underline{M}]$ on the mask, where $\underline{I}$ is the identity matrix. The iterative algorithm of Eq. (5) now becomes

$$\underline{x}(j+1) = \underline{x}(j)\,[\underline{I} - \underline{M}] + \underline{y}\,.$$

For the specific case chosen, we used $P_1 = 0.1$ watts and $N_r = 0.5$ watts (these N_r and P_1 values ensure convergence, and thus the acceleration factor can be unity) and chose θ_1 such that $\lambda = 4\pi/3$. The required matrix mask is thus

$$[\underline{I} - \underline{M}] = \begin{bmatrix} 0.4 & 0.1\exp(-j4\pi/3) \\ 0.1\exp(j4\pi/3) & 0.4 \end{bmatrix}. \tag{14}$$

To realize the complex mask transmittance in Eq. (14), we introduce an alternate technique[18] in which a complex-valued number m′ (one component of the mask) is represented by three real and positive components (m_0', m_1', and m_2') which are the projections of the mask elements along axes at angles 0°, 120°, and 240° in complex space, i.e.,

$$m' = m_0' \exp(j0) + m_1' \exp(j2\pi/3) + m_2' \exp(j4\pi/3) \ . \tag{15}$$

For the specific matrix in Eq. (14), the phase angles of its four components are 0°, 120°, and 240°, and thus we can represent Eq. (14) by the three matrices

$$[\underline{I} - \underline{M}]_0' = \begin{bmatrix} 0.4 & 0 \\ 0 & 0.4 \end{bmatrix}, \quad [\underline{I} - \underline{M}]_1' = \begin{bmatrix} 0 & 0.1 \\ 0 & 0 \end{bmatrix},$$

$$[\underline{I} - \underline{M}]_2' = \begin{bmatrix} 0 & 0 \\ 0.1 & 0 \end{bmatrix} . \tag{16}$$

We note that each of these matrices and all of their elements are positive. As the mask used at P_2 of Fig. 2, we thus spatially multiplexed these three matrices, and as the formatted matrix mask we used

$$[\underline{I} - \underline{M}] = \left[\begin{array}{cc|cc|cc} 0.4 & 0 & 0 & 0 & 0 & 0.1 \\ 0 & 0.4 & 0.1 & 0 & 0 & 0 \\ \hline 0 & 0.1 & 0.4 & 0 & 0 & 0 \\ 0 & 0 & 0 & 0.4 & 0.1 & 0 \\ \hline 0 & 0 & 0 & 0.1 & 0.4 & 0 \\ 0.1 & 0 & 0 & 0 & 0 & 0.4 \end{array}\right] . \tag{17}$$

For the case of two adaptive antenna elements, there will be two complex-valued weights. We represent these by w_a and w_b. Each of these weights will have three positive-valued elements with a decomposition similar to that used in Eq. (15); i.e., for w_a, its three positive projections are w_{a0}', w_{a1}', and w_{a2}', with a similar notation for w_b. The input vector $\underline{w}$ to the first six LEDs is formatted in terms of the six positive numbers corresponding to the three projections of each of the two adaptive weights as

$$\underline{w} = [w_{a0}, w_{b0}, w_{a1}, w_{b1}, w_{a2}, w_{b2}]^T \ . \tag{18}$$

The mask was arranged as described by Eq. (17), the input vector was formatted as described by Eq. (18), and the steering vector was chosen to be

$$\underline{s}^* = [0.3, 0.3]^T \tag{19}$$

for our experiments. The coefficients in the steering vector in Eq. (19) were chosen to simplify the solution. This steering vector corresponds to the boresight direction. Solving Eq. (4) for this case, we find

$$\underline{w} = (0.3/0.35)\left[0.6 - 0.1\exp(-j\pi/3),\right.$$
$$\left. 0.6 - 0.1\exp(+j\pi/3)\right]^T \ . \tag{20}$$

In Fig. 3, we show the outputs from the six relevant photodetector elements of concern in the output of Fig. 2 at iterations j = 0, 1, and 5. In Fig. 3, the six photodetector outputs shown correspond *right-to-left* to the six w components in Eq. (18). The six measured output voltages after the sixth iteration were found to be

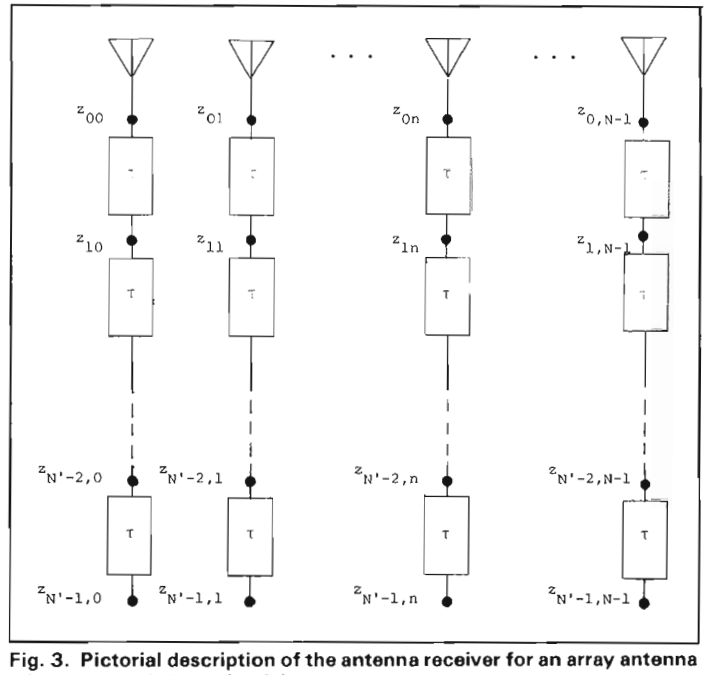

Fig. 3. Pictorial description of the antenna receiver for an array antenna with space and time adaptivity.

$$[0.5118, 0.5118, 0.0834, 0, 0, 0.0834] \ . \tag{21}$$

These compare very well to the exact results in Eq. (20) after an infinite number of iterations. In the order and format in Eq. (18), these exact results are

$$[0.5142, 0.5142, 0.0857, 0, 0, 0.0857] \ . \tag{22}$$

Comparing (21) and (22), we find that the IOP's experimentally calculated weights are within about 1% of the exact values. Thus, the performance of this optical processor appears to be excellent for this simple initial example.

5. MULTIDIMENSIONAL ADAPTIVITY

We now consider extending our adaptive antenna theory of Sec. 2 to include adaptivity in velocity or time (further extensions such as polarization and multipath compensation are possible using the techniques to follow, but the details of such formulations are beyond the present scope of this paper). The adaptive weights $\underline{w} = \{w_n\}$ described in Sec. 2 only affect the spatial frequency response of the antenna and hence the angular position of nulls in the antenna pattern. To control the temporal frequency response of the array, we require taps on the time-history outputs from each antenna element. In Fig. 3, we show a 2-D space-time antenna array. There are N antenna elements and N spatial weights as before. These provide adaptivity in space or in angle. To provide temporal frequency control, we include N′ taps on each antenna element with time delays τ between each. We choose τ to satisfy $\tau = \lambda_R/4v_{max}$, where v_{max} is the blind speed of the radar (i.e., the maximum uniquely resolvable velocity of an object moving relative to the antenna). These provide adaptivity in time or target frequency or velocity. The processor for such an adaptive antenna thus requires the calculation and application of N×N′ weights $w_{n,n'}$ at the $z_{n,n'}$ tap points shown in Fig. 3. We first formulate the required processing as a 2-D extension of the theory of Sec. 2. We then provide an experimental demonstration of the IOP in the solution of such a problem and an analysis of the accuracy of the results obtained (Sec. 6).

We describe this multidimensional adaptive antenna problem by extending our model and analysis of Sec. 2 to include a target or signal at θ_0 with a velocity v_0 and M interference sources at angles θ_m

with M velocities $v_1, \ldots, v_M$. The output at the (n, n') element of the antenna in our 2-D model of Fig. 3 is thus

$$z_{n,n'}(t) = s(t)\, e^{j[\omega t + \pi n \sin\theta_0 + \pi(4\tau/\lambda_R) n' v_0]} + \sum_{m=1}^{M} r_m(t)\, e^{j[\omega t + \pi n \sin\theta_m + \pi(4\tau/\lambda_R) n' v_m]} , \quad (23)$$

where $-\pi/2 < \theta < \pi/2$ and $-(4\tau/\lambda) < v < (4\tau/\lambda)$. The output from the receiver is now more complex than in Eq. (2) and is a 2-D summation given by

$$v_{out}(t) = \sum_{n=0}^{(N-1)} \sum_{n'=0}^{(N'-1)} z_{n,n'}(t)\, w_{n,n'} . \quad (24)$$

The weights are now a 2-D function $w_{n,n'}$. They satisfy the more complex system of linear algebraic equations

$$s^*_{k,k'} = \sum_{n=0}^{(N-1)} \sum_{n'=0}^{(N'-1)} m_{k,k',n,n'} w_{n,n'} , \quad (25)$$

where $m_{k,k',n,n'}$ in Eq. (25) describes the elements of the new covariance matrix $\underline{\underline{M}}$ for the signals in Eq. (23) and where the steering vector is now

$$s^*_{k,k'} = e^{-j\pi[k \sin\theta_0 + (4\tau/\lambda_R) k' v_0]} . \quad (26)$$

Equation (25) is in the general form of a matrix-matrix equation. Since the IOP (Sec. 3) can perform only matrix-vector multiplications, we must convert Eq. (25) into the form of a matrix-vector equation. We achieve this by performing a lexicographic mapping of the 2-D antenna outputs in Eq. (23) onto a vector $\underline{\tilde{z}}(t) = \{z_\ell(t)\}$. For a two-element antenna (N = 2) with two taps (N' = 2) per element, we can relate $\underline{\tilde{z}}$ to the elements $z_{n,n'}$ of $\underline{z}$ by

$$\begin{aligned} \tilde{z}_0(t) &= z_{00}(t) \\ \tilde{z}_1(t) &= z_{01}(t) \\ \tilde{z}_2(t) &= z_{10}(t) \\ \tilde{z}_3(t) &= z_{11}(t) . \end{aligned} \quad (27)$$

We describe a new covariance matrix $\underline{\underline{\tilde{M}}}$ in terms of $\underline{\tilde{z}}$ and a new steering vector $\underline{\tilde{s}}$ that is ordered similar to $\underline{\tilde{z}}$. The resultant weights to be computed are similarly ordered and denoted by $\underline{\tilde{w}}$. With this new notation, we solve the new matrix-vector equation

$$\underline{\tilde{s}}^* = \underline{\underline{\tilde{M}}}\, \underline{\tilde{w}} , \quad (28)$$

where $\underline{\tilde{s}}$ and $\underline{\tilde{w}}$ are lexicographically ordered and where $\underline{\underline{\tilde{M}}}$ is the covariance matrix of the similarly lexicographically ordered received signals $\underline{\tilde{z}}$ in Eq. (27). The solution of Eq. (28) on the IOP of Fig. 2 now follows directly. The space bandwidth product required for the input LEDs, the mask, and the output detector are increased by the lexicographic ordering used. If this becomes prohibitive, one can operate the system successively with one column vector for one of the 2-D functions being the input at successive cycles. This alternate technique for performing matrix-matrix multiplication on a matrix-vector processor was detailed earlier in Ref. 19.

6. MULTIDIMENSIONAL ADAPTIVITY USING THE IOP

In this section, we provide an experimental demonstration of the use of the IOP for multidimensional antenna processing as formulated in Sec. 5. We also emphasize the accuracy of the resultant system with attention to the error source model formulated for the IOP in Sec. 3. We use two performance measures to describe the performance obtained from our adaptive radar processor. Our first performance measure used is the SNR of the resultant antenna pattern. For the spatially-adaptive antenna, the SNR of the output is

$$SNR(j) = \frac{P_0 |E(\theta_0, j)|^2}{\sum_{m=1}^{M} P_m |E(\theta_m, j)|^2} , \quad (29)$$

where P_0 is the strength of the signal located at θ_0, and P_m is the strength of the interference source at θ_m. For the spatially adaptive antenna (Sec. 2), the output antenna pattern E is a function of angle and the iteration number j. The numerator in Eq. (29) describes the total power in the antenna pattern at the location θ_0 of the source, and the denominator is the sum of the total power in the antenna pattern at the location of the M noise sources after application of the adaptive weights. For the multidimensional antenna with adaptivity in space θ and time (or velocity v), the output SNR is a function of the iteration number j as well as angle θ and velocity v. It is described by

$$SNR(j) = \frac{P_0 |E(\theta_0, v_0, j)|^2}{\sum_{m=1}^{M} P_m |E(\theta_m, v_m, j)|^2} , \quad (30)$$

As our second performance measure, we use the processing gain (PG) defined as

$$PG(j) = SNR(j)/SNR(0) . \quad (31)$$

The denominator in Eq. (31) describes the initial output SNR with no adaptive weighting (i.e., after iteration j = 0). The numerator denotes the SNR that results after j iterations. This PG parameter is thus a measure of the output SNR improvement obtained after j iterations. We expect it to increase with j. It is thus most useful in providing a measure of how various choices of the signal and noise scenario and the acceleration parameter ω affect the speed with which our iterative algorithm achieves convergence or a given performance (i.e., a prespecified antenna pattern SNR). To graphically present our results, we will plot the output antenna pattern obtained for the adaptive weights calculated from the IOP. We also compute the output SNR and PG defined above for each of the resultant antenna patterns as a function of the iteration index j and other system and scenario parameters of concern.

We first consider the effect of the acceleration parameter on the number of iterations required for the algorithm to converge to its steady-state value and on the performance obtained after a given number of iterations j. As our performance measure, we use PG(j) in Eq. (31), where this PG represents the amount by which the various interference sources are nulled by our adaptive algorithm. We found this to be a function of the strength P_m of the interference sources (for a fixed antenna or receiver noise N_r and signal strength P_0). To determine the importance of using Eq. (10) for the acceleration parameter rather than $\omega = 1$ as we used in Eq. (14), we considered various signal powers P_0, interference source powers P_m (we consider only one noise source of power P_1), and antenna or receiver noise powers N_r. In Fig. 4, we highlight our results by plotting PG versus the iteration index j for the two different acceleration parameter measures $\omega = 1$ and $\omega = ||\underline{\underline{H}}||^{-1}$. In Fig. 4(a), we consider the case when $P_1 \gg P_0 = N_r$, and in Fig. 4(b), we consider the case when $P_1 = P_0 = N_r$. These data (and much additional testing not included in these drawings) show that SNR increases as in the interference power P_1 is increased with a null depth of 40 dB obtained for a noise source of strength $P_1 = 0.1$ [Fig. 4(a)] and a much poorer 9 dB null depth obtained for a noise source of lower strength $P_1 = 0.001$ [Fig. 4(b)]. This is in agreement with the general performance of an

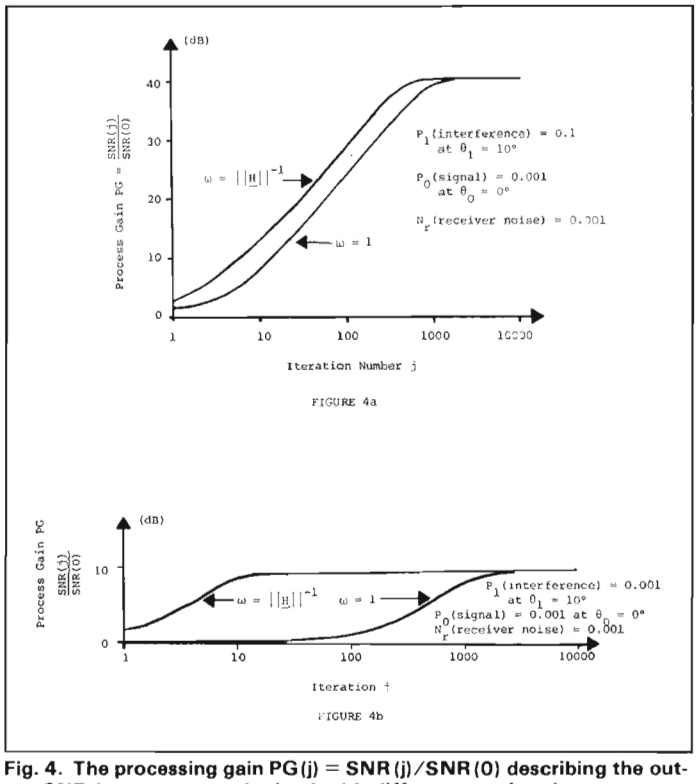

Fig. 4. The processing gain PG(j) = SNR(j)/SNR(0) describing the output SNR improvement obtained with different acceleration parameter choices as a function of the number of iterations j: (a) interference power $p_1 = 0.1$ watts; (b) interference power $p_1 = 0.001$ watts.

adaptive antenna, which provides deeper antenna pattern nulls for stronger interference sources than for weaker ones. From Fig. 4, we also note that the use of our acceleration parameter choice in Eq. (10) becomes increasingly important as the SNR at the input (P_0/P_1) increases and as P_1/N_r increases. This is in agreement with standard adaptive array antenna theory.[1-5] From Fig. 4(b), we notice that our adaptive algorithm converges to the final value in about ten iterations when the acceleration parameter is chosen according to Eq. (10), whereas over 100 times more iterations are needed if no acceleration parameter ($\omega = 1$) is used. Thus, to accommodate all possible ratios of signal, interference, and receiver noise, the use of Eq. (10) for the acceleration parameter is warranted.

In other tests, we studied how the processing gain varied with the angular separation between the signal and the interference source. We verified that our system could achieve super-resolution beyond the classical resolution limit as described further in Ref. 20. When the number of interference sources M is larger than the number of adaptive elements, we found that choosing the locations of the adaptive elements to be randomly distributed on the N×N′ grid in Fig. 3 improves performance very well.

One of our most important theoretical analysis and simulation results concerns the effect of the system's spatial Δb and temporal Δt errors on SNR of the output. We considered an N = 5 element antenna with receiver noise $N_r = 0.1$ and one interference source at $\theta_1 = 45°$ with $P_1 = 1.0$. In Fig. 5, we show SNR(j) as a function of the iteration index j for different Δb and Δt percent errors and noise. With no errors, a steady-state SNR of 44 dB was achieved after about 100 iterations. With a 2.5% spatial error and an 0.5% temporal error ($\Delta b = \pm 0.025$, $\Delta t = \pm 0.005$), we find less SNR than the ideal system can provide, but the SNR is still a very respectable 38 dB value after only 100 iterations. For increased spatial and temporal errors, the system's SNR performance is degraded even worse. The error values included in Fig. 5 are comparable to what the present laboratory IOP system can achieve, and, as seen, its performance is quite acceptable. To obtain the data in Fig. 5, we employed a random number generator with a uniform density function to produce mask errors and detector noise with the three-sigma variance value shown. Different sample realizations of each of these errors were added on each iteration of the IOP. The data in Fig. 5 are the average of five Monte Carlo runs.

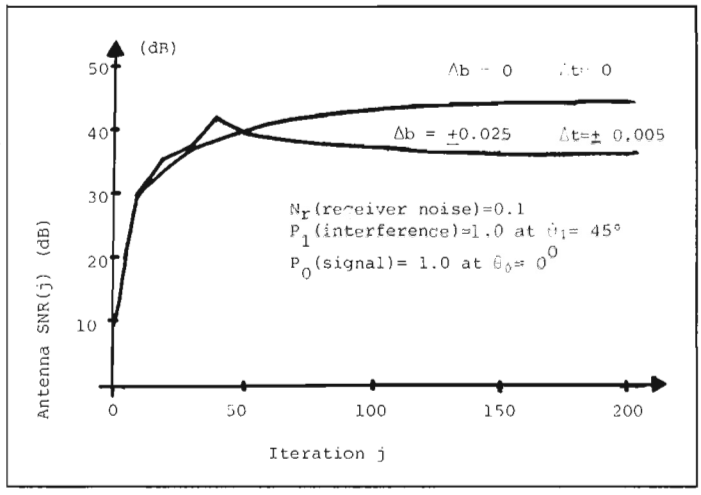

Fig. 5. Output antenna pattern SNR(j) as a function of the number of iterations j for no IOP system errors (Δb = Δt = 0) and for typical experimental IOP errors (Δb = 0.025, Δt = 0.005).

We conclude this section with a detailed description of a typical multidimensional adaptive antenna processing experiment performed on the laboratory IOP. For this case, we consider an N = 2 element array with N′ = 2 time taps. The signal source was of power $P_0 = 0.1$ and located at $\theta_0 = 45°$ and $v_0 = 0.5 v_{max}$. We used one interference source at $\theta_0 = 0°$ and $v_1 = 0$ with power 1.0. The N×N′ = 4 array elements each with receiver noise power $N_r = 1.0$ were lexicographically ordered as described in Eq. (27). The covariance matrix computed from the received signals for this scenario was

$$\underline{\tilde{M}} \simeq \begin{bmatrix} 2 & 1 & 1 & 1 \\ 1 & 2 & 1 & 1 \\ 1 & 1 & 2 & 1 \\ 1 & 1 & 1 & 2 \end{bmatrix} \tag{32}$$

The Euclidean norm of $\underline{H}$ calculated from Eq. (32) is 7.48. We used its reciprocal as our acceleration parameter $\omega = 0.13$ as described in Eq. (10). The complex-valued format in Eq. (8) was then used for $\underline{M}$.

For this case, $\underline{M}$ is real and thus it is arranged as the 8×8 matrix

$$\underline{\tilde{M}} = \begin{bmatrix} \underline{\tilde{M}}_{re} & \underline{0} \\ \underline{0} & \underline{\tilde{M}}_{re} \end{bmatrix}, \tag{33}$$

where $\underline{\tilde{M}}_{re}$ is described by Eq. (32). To obtain the optical mask used in the actual system, we divided each element of $\underline{\tilde{M}}$ by $(h_{max} - h_{min}) = 2$ and biased the entire matrix by $h_{min}/(h_{max} - h_{min}) = 0$. The resultant optical mask actually placed at P_2 of Fig. 2 was thus

$$\underline{H} = \begin{bmatrix} \underline{H}_{re} & 0 \\ 0 & \underline{H}_{re} \end{bmatrix}, \tag{34}$$

Where $\underline{H}_{re}$ is the same $\underline{\tilde{M}}_{re}$ in Eq. (32) with each element divided by two. The complex-valued steering vector corresponding to the signal direction $\theta_0 = 45°$ and $v_0 = 0.5$ has element values given by Eq. (26). When arranged in the lexicographic format of Eq. (27), it becomes

$$\underline{\tilde{s}}^* = \begin{bmatrix} -0.82 - 0.61j \\ 0.97 - 0.27j \\ 0.61 - 0.82j \\ 0.27 + 0.97j \end{bmatrix} . \quad (35)$$

We easily decompose Eq. (35) into its real and imaginary parts and obtain the eight element exogenous vector

$$\underline{y} = [\underline{s}^*_{re}\ \underline{s}^*_{im}]^T = [-0.82, 0.97, 0.61, 0.27, -0.61 , -0.27, -0.82, 0.97]^T . \quad (36)$$

The two cycle complex algorithm described in Sec. 3 was employed with the positive elements of $\underline{y}$ used on odd iterations and the negative elements on even iterations. The $\underline{x}$ outputs were computed by the laboratory IOP for the first fifty iterations. The microprocessor support system and the dedicated high speed memory in the IOP were used to combine the positive and negative outputs from successive iterations and to store the resultant bipolar numbers $\underline{w}(j)$ computed at each iteration j. The eight relevant photodetector outputs corresponding to the eight elements of the bipolar and complex-valued output vector $\underline{x} = [\underline{x}^*_{re}\ \underline{x}^*_{im}]$ corresponding to the complex-valued weights $\underline{w}$ are shown in Fig. 6 after the first, fifth, and fiftieth iterations. We denote these outputs by $\underline{x}(1)$, $\underline{x}(5)$, and $\underline{x}(50)$, respectively, in the Fig. 6 caption. The complex-valued weights

$$\underline{w} = \underline{w}_{re} + j\underline{w}_{im} = [w_{00}, w_{10}, w_{01}, w_{11}]^T \quad (37)$$

were directly obtained from the eight $\underline{x}$ outputs $(\underline{x}_1, \ldots, \underline{x}_8)$ according to

$$\begin{aligned} W_{00} &= x_1 + jx_5 \\ W_{10} &= x_2 + jx_6 \\ W_{01} &= x_3 + jx_7 \\ W_{11} &= x_4 + jx_8 \end{aligned} \quad (38)$$

After the fiftieth iteration, we obtained

$$\underline{w}(50) = \begin{bmatrix} -0.9 - 0.45j \\ 0.75 - 0.25j \\ 0.4 - 0.8\ j \\ 0.2 + 1.1\ j \end{bmatrix} . \quad (39)$$

To determine the accuracy of these results, we first calculated the rms errors between the exact weights and those computed after 50 iterations. This error was found to be 2.3% (it did not decrease appreciably when further iterations were performed). The true measure of the performance accuracy of the weights computed from the laboratory IOP lies in the SNR obtained in the output pattern that results when the weights in Eq. (39) are applied with the interference sources and receiver noise indicated. The resultant antenna pattern was obtained. Its SNR was 14.7 dB. This is nearly exactly equal to the SNR obtained (14.96 dB) if the exact weights were applied. We thus find the laboratory IOP system to be extremely accurate with less than 0.26 dB difference in the SNR of the output antenna for the cases of the optically computed weights and the exact weights. Initial simulations were performed to verify that these results were typical of those to be expected. The above results were found to be typical for the ten different cases we considered. We also produced initial theoretical expressions[21] from which upper bounds on the performance of the IOP can be predicted as a function of spatial and temporal system errors. In all cases, the results obtained in our experiments were well below the weak bounds we derived. Because of this, no derivation of these bounds is included at present.

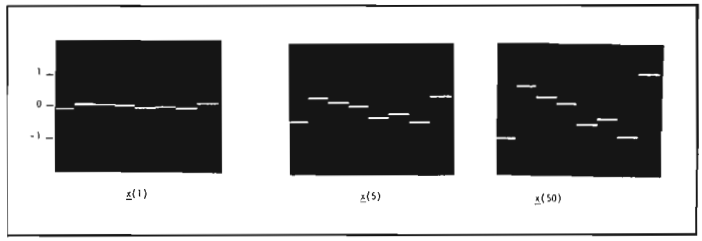

Fig. 6. Experimental outputs from the relevant eight photodetectors of the IOP of Fig. 2 in the computation of the complex-valued weights for a multidimensional antenna with space and time adaptivity.

7. CONCLUSION

We have reviewed the basic signal processing requirements for adaptive antennas and have provided a summary description of an iterative optical matrix-vector processor that appears most attractive for such advanced signal processing applications. Modifications to our initial IOP were described to allow incorporation of an acceleration parameter, and two techniques were described to allow the system to operate on complex-valued data (as required for the APAR application). Theoretical and experimental data and simulations showed that use of an acceleration parameter equal to the reciprocal of the Euclidean norm of the covariance matrix greatly reduced the number of iterations needed (by a factor of 100 or more), especially as the interference power approaches the signal power and the receiver noise. We described and experimentally demonstrated two different techniques by which the system can operate on complex-valued data. The technique (Sec. 4) in which each complex number is represented by its three positive projections on three axes in the complex plane requires more space bandwidth product with fewer iterations. The bipolar technique (Secs. 3 and 6) in which the positive- and negative-valued input data are used on successive iterations requires twice the number of iterations but less space bandwidth product than the technique used in Sec. 4. The choice between these two methods of handling complex-valued data depends upon the number of adaptive weights, the speed required, the space bandwidth product available on the IOP used, and the importance of canceling fixed-pattern detector noise.

We have also extended the use of the system to include multidimensional adaptivity and have experimentally demonstrated angular adaptivity and multidimensional space and time adaptivity on our laboratory IOP. The experimental performance obtained was quite excellent. Theoretical and simulation studies have shown that the performance of the present IOP with its 0.8% spatial errors and 0.4% temporal errors is quite adequate for APAR applications. Our experiments showed an rms error of only 2.3% in the computed weights, and, more important, that this resulted in less than an 0.26 dB difference in the SNR of the output antenna pattern. This novel and most general purpose optical processing architecture merits more research and analysis for the indicated APAR problem and for many other diverse applications that can be reduced to matrix-vector equations and matrix-inversion problems.

8. ACKNOWLEDGMENT

The support of the Air Force Office of Scientific Research on a supplement to Grant AFOSR-79-0091 which enabled us to complete the work herein is gratefully acknowledged.

9. REFERENCES

1. B. Widrow, P. Mantey, L. Griffiths, and B. Goode, Proc. IEEE 55(12), 2143(1967).
2. S. Applebaum, IEEE Trans. Antennas Propag. AP-24 (5), 585(1976).
3. L. Brennan and L. Reed, IEEE Trans. Aerospace and Electronic Systems AES-9 (2), 237(1973).
4. W. Gabriel, Proc. IEEE 64(2), 239(1976).
5. Special Issue on Adaptive Antennas, IEEE Trans. Antennas Propag. AP-24 (1976).
6. D. Casasent, IEEE Commun., 40 (Sep. 1981).
7. M. Carlotto and D. Casasent, Appl. Opt. 21, 147 (Jan. 1, 1982).
8. D. Psaltis, D. Casasent, and M. Carlotto, Proc. SPIE 180, 114(1979).
9. D. Casasent and M. Carlotto, "A Novel Optical Processor for Adaptive Phased Array Radar," Proc. SPIE 341 (May 1982).
10. D. Psaltis, D. Casasent, and M. Carlotto, Opt. Lett. 4, 348 (Nov. 1979).
11. A. Edison and M. Noble, "Optical Analog Matrix Processors," AD646060 (Nov. 1966).
12. P. Mengert et al., U.S. Patent 3,525,856 (Oct. 6, 1966).
13. J. Goodman, A. Dias, and L. Woody, Opt. Lett. 2, 1(1978).
14. L. Richardson, *Philos. Trans. R. Soc. London, Ser. A210,* 307(1910).
15. J. Grinberg, W. P. Bleha, P. O. Braatz, K. Chow, D. H. Close, A. D. Jacobson, M. J. Little, N. Massetti, R. J. Murphy, J. G. Nash, and M. Waldner, Proc. SPIE 128, 253(1977).
16. H. Caulfield et al., Opt. Commun. 40, 86(1981).
17. D. Casasent, Appl. Opt. 21, 1859(1982).
18. J. Goodman and L. Woody, Appl. Opt. 16, 2611(1977).
19. D. Casasent and C. Neuman, "Operations Achievable on an Iterative Optical Processor," Proc. NASA Conference on Applications of Optical Processing to Aerospace Needs (Aug. 1981).
20. G. Borgiotti and L. Kaplan, IEEE Trans. Antennas Propag. AP-27 (6), 842(1979).
21. M. Carlotto, "Iterative Electro-Optic Matrix Processor," PhD Thesis, Carnegie-Mellon University (April 1981).